Steering of a 3D Bipedal Robot with an Underactuated Ankle

Christine Chevallereau, J.W. Grizzle, and Ching-Long Shih

Abstract— **This paper focuses on steering a 3D robot while walking on a flat surface. A hybrid feedback controller designed in [1] for stable walking along a straight line is modified so that it is capable of adjusting the net yaw rotation of the robot over a step in order to steer the robot along paths with mild curvature. The controller is designed on the basis of a single pre-defined trajectory for periodic walking along a straight line. In order to illustrate the role of internal/external (i.e., medial/lateral) rotation at the hip in achieving curved walking motions, the performance of two robots, one with internal/external rotation and one without, is compared.**

I. INTRODUCTION

In a previous paper, we addressed the control of a 3D bipedal robot with an unactuated ankle, where the ground contact inhibited yaw motion, but pitch and roll of the stance leg were unconstrained and unactuated [1]. The first objective of the present paper is to present an event-based controller that steers the robot along paths of mild curvature. A novel feature of the solution is that steering is achieved on the basis of a single, predefined, periodic motion corresponding to walking along a straight line. The second objective of the paper is to compare the turning ability of robots with a 2 degree of freedom (DOF) hip joint versus a 3 DOF hip joint.

The ability to turn is an essential feature for stepping around obstacles on a given surface. Honda's ASIMO has demonstrated the important ability to walk forward, backward, right, left, up and down stairs, and on uneven terrain [2]. Very few other works have addressed the issue of a turning motion for bipedal robots, and all addressed models with actuated feet (in particular, full actuation was assumed). Previous techniques on bipedal turning motion include change of the duty ratios of the two legs, allowing the feet to slip when rotating with respect to the ground, reduction and decoupling, and trial-and-error methods [3], [4], [5]. The authors of [6] have developed an elegant and rigorous setting for stable walking and steering of fully actuated 3D robots on the basis of geometric reduction and passivity-based control. The controlled geometric reduction

decouples the biped's sagittal-plane motion from the yaw and lean modes [7]. Steering is achieved by adjusting the yaw set point of the within-stride passivity-based controller.

We study here two 3D biped robots with passive ankles, and seek a time-invariant feedback controller that creates an exponentially stable, periodic walking motion, along with the ability to steer the yaw orientation of the robot with respect to an inertial frame, that is, the robot's direction of travel. The two robots are each equipped with a 2 degree of freedom (DOF) passive ankle, a 1 DOF knee, and differ at the hip, which in one case is a 2 DOF joint and in the other, a 3 DOF joint: one robot's hip allows internal/external (i.e., medial/lateral) rotation, the other one does not. The performance of the two robots is compared in a task that requires steering.

The control approach presented in this paper allows us to change the direction of motion of the robot through the net yaw motion about the stance foot over a step. An event-based (or stride-to-stride) feedback controller distributes set point commands to the actuated joints in order to achieve a desired amount of turning, as opposed to the continuous corrections used in [6].

Section II presents the dynamic model of the biped. Section III summarizes the principle of the within-stride control design used to obtain periodic motion along a straight line; a simulation for the robot with 3 DOF at the hip are shown and it is noted that the yaw motion about the stance foot is unstable under the within-stride controller. In Section IV, a supplemental event-based control law to regulate the direction of motion of the robot is presented. Simulation results are presented for a path following task in Section V. Section VI concludes the paper.

II. MODEL

A simplified model of a spatial bipedal robot is given here. The legs are considered in detail, while the upper body (head, torso and arms) is represented by a single link articulated only at the hip. The feet are massless and unactuated.

A. Description of the robot and the walking gait

The two 3D bipedal robots discussed in this work are depicted in Figure 1. They consist of a torso and two legs with revolute 1 DOF knees that are independently actuated and terminated with massless feet articulated by a 2 DOF ankle. The two robots differ in the number of DOF at the hip. The robot in Figure 1 (a), which was studied in [1], has hips composed of two, one DOF, actuated, revolute joints corresponding to motion in the sagittal and frontal planes. The hip of the second robot depicted in Figure 1 (b) includes

Christine Chevallereau is with the CNRS, IRCCyN, 1 rue de la Noe, 44321 Nantes, cedex 03, France, `Christine.Chevallereau@irccyn.ec-nantes.fr`

Jessy W. Grizzle is with the Control Systems Laboratory, Electrical Engineering and Computer Science Department, University of Michigan, Ann Arbor, MI 48109-2122, USA, `grizzle@umich.edu`.

Ching-Long Shih is with the EE Department, National Taiwan University of Science and Technology, Taipei, Taiwan 106, `shihcl@mail.ntust.edu.tw`

a third actuated DOF corresponding to external/internal rotation. This supplementary rotation could also be added at the ankle instead of the hip, but most humanoid robots include a 3 DOF hip and a 2 DOF ankle. In total, the bipeds in the single support phase have six or eight actuated DOF, and there are two degrees of underactuation in the stance ankle (see Figure 1).

The ankle is composed of two single DOF joints, one in the sagittal plane and the other in the frontal plane. We consider flat-footed walking, and in order to ensure that the ZMP condition is met, namely the ground reaction forces remain with the convex hull of the foot [8], [9], we impose that the torque in the stance ankle be zero[1]. Because the foot is assumed to be massless, during the swing phase, the foot's orientation can be freely chosen and therefore the swing ankle joint is not included in the model, which simplifies the model.

The gait considered in this study consists of two alternating phases of motion: single support and double support. Walking takes place on a flat surface. The double support phase is instantaneous and occurs when the swing leg impacts the ground on a flat foot. The swing and stance legs exchange their roles at each impact.
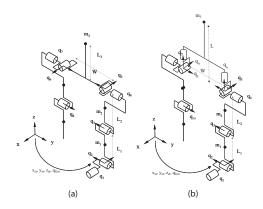

Fig. 1. Two 3D bipeds with massless feet, shown in support on leg-1. The massless swing foot is not included in the model. The stance ankle torques are zero. The robot on the right includes an extra degree of freedom at the hip corresponding to internal/external (i.e., medial/lateral) rotation.

The robot is represented as a tree structure. The stance foot, which is fixed on the ground, is the base of the tree. A set of generalized coordinates $q = [q_1, \ldots, q_n]'$ is shown in Figure 1 with $n = 8$ or $n = 10$. The coordinates (q_1, q_2) are unactuated (due to the assumption of zero torque in the stance ankle), while $(q_3, \ldots, q_n)$ are independently actuated.

The position of the robot with respect to an inertial frame is defined by adding the four variables $x_e = [q', x_{st}, y_{st}, z_{st}, q_{0,st}]'$, where x_{st}, y_{st} and z_{st} are the Cartesian coordinates of the stance foot, and $q_{0,st}$ defines the rotation along the z-axis of the stance leg. These variables are constant during each single support phase.

B. Dynamic model

The Euler-Lagrange equations yield the dynamic model for the robot in the single support phase as

$$D(q)\ddot{q} + H(q, \dot{q}) = B\,u = \begin{bmatrix} 0_{2\times(n-2)} \\ I_{(n-2)\times(n-2)} \end{bmatrix} u, \quad (1)$$

where $D(q)$ is the positive-definite $(n \times n)$ mass-inertia matrix, $H(q, \dot{q})$ is the $(n \times 1)$ vector of Coriolis and gravity terms, B is an $(n \times (n-2))$ full-rank, constant matrix indicating whether a joint is actuated or not, and u is the $((n-2) \times 1)$ vector of input torques. The double support phase is assumed to be instantaneous. However, it actually consists of two distinct subphases: the impact, during which a rigid impact takes place between the swing foot and the ground, and coordinate relabeling. Analogously to [1], the overall impact model can be written as

$$x_e^+ = \Delta_x^e(x_e^-) \quad \text{and} \quad \dot{q}^+ = \Delta_{\dot{q}}(q^-, \dot{q}^-). \quad (2)$$

III. PERIODIC WALKING

A. Virtual constraints

How to define a stable walking gait along a straight line is summarized in this section. The method of virtual constraints has been applied in [1] to stabilize the motion of the 3D robot presented in Figure 1 (a). The virtual constraints can be understood as a parametrization of the desired configuration of the robot throughout a step; in particular, they define the joint path in the configuration space of the robot, but not a joint trajectory. The temporal evolution of the robot is free and determined via the evolution of the zero dynamics.

The method of virtual constraints can also be applied to the robot presented in Figure 1 (b). We assume that a periodic solution of the model, corresponding to walking in a straight line, has been determined, for example, using the method presented in [1]. The objective of the control law is that the robot's trajectories converge to this nominal periodic motion. One holonomic constraint per actuator is proposed in the form of an output that, when zeroed by a feedback controller, enforces the constraint. The outputs are

$$y = q_c - h_c^d(\theta), \quad (3)$$

where

$$q_c = Cq \quad (4)$$

C is a constant $((n-2) \times n)$ matrix that defines the $n-2$ linear combinations of the joint variables that are controlled using the $n-2$ actuators, the quantity $\theta = \theta(q)$ is strictly monotonic (i.e., strictly increasing or decreasing) along a typical walking gait , and $h_c^d(\theta)$ parametrizes the desired evolution of the controlled variables as a function of θ. Assuming that a reference periodic motion $q^*(\theta)$ is known for the configuration vector q, then $h_c^d(\theta) = Cq^*(\theta)$.

Let $q_u = [q_1, \theta]'$ denote the unactuated joints, and q_c denote the controlled joints. A linear relation exists between q_c, q_u and q,

$$q = \mathcal{T} \begin{bmatrix} q_u \\ q_c \end{bmatrix}, \quad (5)$$

where we assume that the controlled variables, chosen via C in (4), are such that $\mathcal{T}$ is an $(n \times n)$ invertible matrix.

B. The control law

For a given vector of constraints (3), a feedback controller in the single support phase that drives or maintains the state of the robot on the constraint surface corresponding to $q_c = h_c^d(\theta)$ can be determined [10]. The control law is such that, on the periodic orbit, the virtual constraints (3) are identically satisfied and the state of the robot belongs to $Z = \{(q, \dot{q}) | y(q) = 0, \ \dot{y}(q) = 0\}$. However, off the periodic orbit, even if the virtual constraints are satisfied at the end of given step, they will not in general be satisfied at the beginning of the next step, and hence the surface Z is not invariant under the hybrid dynamic model (1) and (2). Consequently, the simulation of the complete model is required in order to predict the evolution of the robot.

Following [1], the virtual constraints are modified stride to stride so that they are compatible with the initial state of the robot at the beginning of each step, thereby recovering invariance and creating a hybrid zero dynamics. The new output for the feedback control design is

$$y_c = h(q, y_i, \dot{y}_i) = q_c - h_c^d(\theta) - h_m(\theta, y_i, \dot{y}_i). \quad (6)$$

This output consists of the previous output (3), and a correction term h_m that depends on (3) evaluated at the beginning of the step, specifically, $y_i = q_{c,i} - h_c^d(\theta_i)$ and $\dot{y}_i = \dot{q}_{c,i} - \frac{\partial h_c^d(\theta)}{\partial \theta}\dot{\theta}_i$, where the subscript "$i$" denotes the initial value for the current step. The values of $y_i, \dot{y}_i$ are updated at the beginning of each step. The function h_m is taken as:

$$\begin{cases} h_m(\theta_i, y_i, \dot{y}_i) & = & y_i \\ \frac{\partial h_m}{\partial \theta}(\theta_i) & = & \frac{\dot{y}_i}{\dot{\theta}_i} \\ h_m(\theta, y_i, \dot{y}_i) & \equiv & 0, \quad \frac{\theta_i + \theta_f}{2} \leq \theta \leq \theta_f. \end{cases} \quad (7)$$

With h_m designed in this way, the output and its derivative are smoothly joined to the original virtual constraint by the middle of the step. In particular, for any initial error, the initial virtual constraint h_c^d is exactly satisfied for $\theta \geq \frac{\theta_i + \theta_f}{2}$ (see Figure 4).

C. Stability test

The next objective is to determine the behavior of the robot under the virtual constraints. This task is simplified by noting that enforcing the virtual constraints, $y = 0$, results in $q_c = h_c^d(\theta) + h_m(\theta_i, y_i, \dot{y}_i)$ and reduces the dimension of the dynamics.

Using (5), the dynamic model in single support (1) can be rewritten as

$$\mathcal{T}'D(q)\mathcal{T}\begin{bmatrix} \ddot{q}_u \\ \ddot{q}_c \end{bmatrix} + \mathcal{T}'H(q,\dot{q}) = \begin{bmatrix} 0_{2\times(n-2)} \\ I_{(n-2)\times(n-2)} \end{bmatrix} u. \quad (8)$$

The first two rows of the right hand side of this equation are zero, yielding

$$D_{11}(q)\ddot{q}_u + D_{12}(q)\ddot{q}_c + H_1(q,\dot{q}) = 0_{2\times 1}, \quad (9)$$

where D_{11} is the (2×2) upper left sub-matrix of $\mathcal{T}'D(q)\mathcal{T}$, D_{12} is the $(2\times(n-2))$ upper right sub-matrix of $\mathcal{T}'D(q)\mathcal{T}$ and $H_1(q,\dot{q})$ consists of the first two rows of $\mathcal{T}'H(q,\dot{q})$.

Next, the expression for q_c when the constraint is satisfied, $q_c = h_c^d(\theta) + h_m(\theta_i, y_i, \dot{y}_i)$, is used. Substituting this relation into (9), the dynamic model of the single support phase is now reduced to a 2-DOF, autonomous system, which is called the zero dynamics [10].

$$D_{11}(q_u)\begin{bmatrix} \ddot{q}_1 \\ \ddot{\theta} \end{bmatrix} + H_1(q_u, \dot{q}_u) +$$
$$D_{12}(q_u)\left((\frac{\partial h_c^d}{\partial \theta} + \frac{\partial h_m}{\partial \theta})\ddot{\theta} + (\frac{\partial^2 h_c^d}{\partial \theta^2} + \frac{\partial^2 h_m}{\partial \theta^2})\dot{\theta}^2 \right) = 0_{2\times 1}, \quad (10)$$

The stability of a fixed-point x^* can now be tested numerically using a restricted Poincaré map defined with any Poincaré section transversal to the periodic orbit. In this study, the Poincaré section will be defined by $S = \{(q, \dot{q}) \mid \theta = \frac{\theta_i + \theta_f}{2}\}$, where θ_i and θ_f are the initial and final values of θ on the periodic orbit, respectively. In $S \cap Z$, the state of the robot can be represented using only three independent variables, $x^z = [q_1, \dot{q}_1, \dot{\theta}]'$.

The restricted Poincaré map $P^z : S \cap Z \rightarrow S \cap Z$ induces a discrete-time system $x_{k+1}^z = P^z(x_k^z)$. From [11], *the linearization of P^z about a fixed-point x^{z*} determines the exponential stability of the full-order closed-loop robot model.* Define $\delta x_k^z = x_k^z - x^{z*}$. The Poincaré map linearized about a fixed-point $x^{z*} = (q_1^*(\frac{\theta_i + \theta_f}{2}), \dot{q}_1^*(\frac{\theta_i + \theta_f}{2}), \dot{\theta}^*(\frac{\theta_i + \theta_f}{2}))$ gives rise to a linearized system,

$$\delta x_{k+1}^z = A^z \delta x_k^z, \quad (11)$$

where the (3×3) square matrix A^z is the Jacobian of the Poincaré map. A fixed-point of the restricted Poincaré map is locally exponentially stable, if, and only if, the eigenvalues of A^z have magnitude strictly less than one [10, Chap. 4].

D. An example of stable walking

For the model presented in Figure 1 (a), a stable walking gait is presented in [1]. For the model presented in Figure 1 (b), a periodic reference motion q^* is presented in the stick diagram of Figure 2. The outputs are chosen as $y_i = q_{i+2} - q_{i+2}^*(\theta) + a_i(q_1 - q_1^*(\theta))$ for i=1,8, with $a_1 = a_2 = a_4 = a_5 = a_7 = a_8 = 0$, $a_3 = 1.7$ and $a_6 = 1.2$. A stable gait is obtained, with the eigenvalues of A^z being $\lambda_1 = 0.5950$, $\lambda_{2,3} = 0.2921 \pm 0.6259i$.
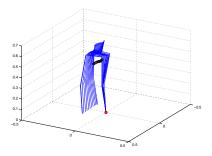

Fig. 2. The stick diagram for robot presented in 1 (b) and the periodic reference motion studied.

- To illustrate the orbit's local exponential stability, the 3D biped's model in closed-loop is simulated with the initial state perturbed from the fixed-point x^*. An initial error of

$-0.5°$ is introduced on each joint and a velocity error of $+2°s^{-1}$ is introduced on each joint velocity. All the variables q converge to their desired cyclic motion.

Figure 3 shows the evolution of values of the three independent variables describing the evolution of the robot on the restricted Poincaré section $S \cap Z$. These variables clearly converge to the periodic motion. The lower-right figure shows the evolution of $q_{0,st}$, which represents the orientation of the stance foot in an absolute frame, and hence the direction of motion of the robot. For a walking motion along the x-axis, the nominal value of $q_{0,st}$ on the periodic orbit is $\pm 4.e - 5$ rad. It can be seen that due to the transients induced by the initial errors, even if the initial value of $q_{0,st}$ is the nominal value, the direction of motion of the robot will be different from zero. From a practical point of view, it is important to be able to control the direction of motion of the robot; the stability of the gait is not enough.
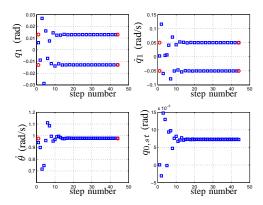

Fig. 3. The evolution of the three independent variables describing the evolution of the robot on the restricted Poincaré section $S \cap Z$, with the initial condition perturbed from x^*. The fourth graphic shows the evolution of $q_{0,st}$, which represents the yaw orientation of the stance foot in an absolute frame.

IV. CONTROL OF THE DIRECTION OF MOTION

A. Preliminaries

In order to be able to control the direction of the robot, we will consider an extended set of configuration variables, $q_e = [q', q_{0,st}]'$, obtained by appending the robot's direction of motion to the previous model. The control of this extended system can be studied as in Sec. III. The extended restricted Poincaré map is studied using the four independent variables $x^e = [q_1, \dot{q}_1, \dot{\theta}, q_{0,st}]'$. The corresponding linearized extended restricted Poincaré map is written as

$$\delta x^e_{k+1} = A^e \delta x^e_k, \qquad (12)$$

where A^e is a (4×4) matrix.

The equations of motion of the robot during single support are independent of $q_{0,st}$; moreover, $q_{0,st}$ is constant[2] as it evolves only during the impact phase (2)[3]. In [12], it

[2]This is because we have assumed no yaw rotation at the stance foot.

[3]After impact, the parametrization of the robot is modified in order to take into account that the first joint of the robot corresponds to the stance leg. In this relabeling, the variables x_e undergo a jump. Thus the jump of $q_{0,st}$ is a direct function of the impact configuration.
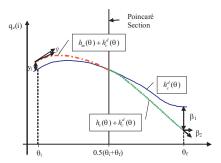
is shown that the impact surfaces are invariant under the rotation around the z-axis of the absolute frame, and the impact maps are equivariant under this rotation

$$x^+_e + q_{0,st}e_0 = \Delta^e_x(x^-_e + q_{0,st}e_0), \qquad (13)$$

where $e_0 = [0, ..., 0, 1]'$ is the unity vector corresponding to the configuration variable $q_{0,st}$. As a consequence, the linearized extended restricted Poincaré map has the same property

$$\delta x^e_{k+1} + q_{0,st}e_0 = A^e(\delta x^e_k + q_{0,st}e_0), \qquad (14)$$

where e_0 is defined here as $e_0 = [0, 0, 0, 1]'$.

Thus the fourth column of A^e is $[0, 0, 0, 1]'$, and the additional eigenvalue is $\lambda_4 = 1$. This is a property of the model of the robot and is independent of the choice of the controlled output. It follows that the direction of motion cannot be controlled by the strategy proposed in Sec. III.

A second conclusion of (14) is that an infinite number of fixed points exist: if x^{e*} is a fixed point (for us, x^{e*} denotes the fixed point corresponding to a robot motion aligned the axis x), $x^{e*} + q_{0,st}e_0$ is also a fixed point. Thus an infinite number of periodic walking gaits exist, one for each direction of motion. If a control strategy can be devised such that the robot converges to a motion with a desired direction of travel, $x^{e*} + q^d_0 e_0$, then the direction of the robot can be steered by changing q^d_0.

B. Control of the robot's direction

An event-based controller [13] is integrated with the continuous, stance phase controller to regulate the direction of travel $q_{0,st}$. Let β be a vector of parameters that affect the desired reference trajectory. The parameters will be modified at $\theta = \frac{\theta_i + \theta_f}{2}$, where they will be updated on the basis of the state of the extended hybrid zero dynamics in order to achieve convergence to a desired fixed point $x^{e*} + q^d_0 e_0$. Here our main objective is to control $q_{0,st}$, which evolves at impact only. Thus a natural modification of the periodic reference trajectory is to change the impact configuration. In order to provide more degrees of freedom and to accelerate the convergence, a modification of the desired velocity at the end of the single support phase is also considered.

The output in (6) is augmented with an additional term $h_s(\theta, \beta)$ depending on $\beta = [\beta^1, \beta^2]$, yielding

$$y = q_c - h^d_c(\theta) - h_m(\theta, y_i, \dot{y}_i) - h_s(\theta, \beta), \qquad (15)$$

with

$$\begin{cases} h_s(\theta_f, \beta) &= \beta^1 \\ \frac{\partial h_s}{\partial \theta}(\theta_f, \beta) &= \beta^2 \\ h_s(\theta, \beta) &\equiv 0, \ \theta \le \frac{\theta_i + \theta_f}{2}. \end{cases} \qquad (16)$$

In spite of the term h_s, the control law of Sec. III will still create a hybrid zero dynamics. This is because the parameters in h_m are updated at the beginning of the step, while the updates to β in h_s are done at $\theta = \frac{\theta_i + \theta_f}{2}$ and because h_s modifies the reference trajectory only between $\theta = \frac{\theta_i + \theta_f}{2}$ and the impact. The modification of the reference path is illustrated in Figure 4.

Fig. 4.   The initial reference path $h_c^d(\theta)$ is modified via h_m to create an invariant surface and by h_s to steer the robot. The restricted Poincaré section $S \cap Z$ is chosen in order to preserve the initial fixed point $x^{z*} = (q_1^*(\frac{\theta_i + \theta_f}{2}), \dot{q}_1^*(\frac{\theta_i + \theta_f}{2}), \dot{\theta}^*(\frac{\theta_i + \theta_f}{2}))$ in the presence of the modifications h_m and h_s.

The Poincaré map can now be viewed as a nonlinear control system with inputs β_k, $x_{k+1}^e = P(x_k^e, \beta_k)$, where β_k is the value of β during the second part of step k. Linearizing this nonlinear system about any fixed point $x^{e*} + q_0^d e_4$ (since this model does not depend on $q_{0,st}$) and the nominal parameter value $\beta^* = 0_{(2n-4) \times 1}$ leads to

$$\delta x_{k+1}^e = A^e \delta x_k^e + F \delta \beta_k, \qquad (17)$$

where $\delta x_k^e = x_k^e - (x^{e*} + q_0^d e_0)$, $\delta \beta_k = \beta_k - \beta^*$, and F is the Jacobian of P with respect to β. Designing a feedback law

$$\delta \beta_k = -K \delta x_k^e \qquad (18)$$

such that the eigenvalues of $(A^e - FK)$ have magnitude strictly less than one will exponentially stabilize the fixed point $x^{e*} + q_0^d e_0$.

When the $((2n-4) \times 4)$ gain matrix K is calculated via a DLQR technique, the eigenvalues become $\lambda_1 = 0.6421$, $\lambda_{2,3} = -0.2491 \pm 0.0732i$, and $\lambda_4 = 0.0371$.

To illustrate the effect of this modification of the control strategy on the robot's behavior, the 3D biped's model in closed-loop is simulated with the initial state perturbed from the fixed-point x^{e*}. An initial error of $-0.5°$ is introduced on each joint and a velocity error of $+2°s^{-1}$ is introduced on each joint velocity. The initial yaw angle of the stance foot is $3°$ with a desired average direction of motion of $0°$.

Figure 5 shows the center of mass and the position of the feet on the ground. The direction of the walking motion is controlled, and the robot evolves along a path parallel to the x-axis, but an offset of the robot's motion with respect to its initial position can be seen in the y-direction.
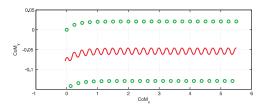

Fig. 5.   The evolution of the projection the robot's center of mass of the robot on the ground is shown by the red line, and the position of the feet on the ground is shown by the green circles.

V. CONTROL OF THE ROBOT'S PATH

A. Method

A common objective of a walking robot is to reach a given location from an initial point. For example, in a home, the robot may need to move from one room to another by passing through a door. This requires more precise control than just orientation, as the robot's path must pass through the door. Figure 6 introduces parameters that will be used to describe the desired motion of the robot in order to regulate its path: the initial pose of the robot is d_i, q_{0i} and the desired pose is $d = 0$, $q_0 = 0$, the distance along x is not prescribed.
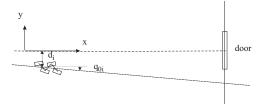

Fig. 6.   The robot begins its motion at a pose defined by d_i, q_{0i}. d_i is the distance along the y-axis of the middle of the two ankles at impact. The robot's task is to asymptotically join the path defined by $d = 0$, $q_0 = 0$ as x increases.

In human walking, it has been observed that, in the majority of turning methods, a person behaves like a nonholonomic vehicle: when the goal is far, a lateral step is not used to achieve lateral displacement, rather continuous modification of walking direction (i.e., orientation) is used to produce smooth lateral displacement [14]. Thus it is natural to use the orientation of the robot in order to control its motion along a desired path. A high-level supervisory controller can be integrated into the overall controller to resolve this problem. From one step to the next, the evolution of the pose of the robot will be modeled as

$$\begin{aligned} d_{k+1} &= d_k + l \sin(q_{0k}) \\ q_{0k+1} &= q_{0k} + \delta q_0, \end{aligned}$$

which assumes that the step length l and step width are constant.

The change of orientation δq_0 will be implemented through a change of the desired fixed point $x^{e*} + q_0^d e_0$. To avoid slipping, collision with the ground, or other physical constraints, δq_0 must not be too large. Hence, at step k, the desired fixed point is chosen as $x^{e*} + (q_{0k} + \delta q_0)e_0$, where

$$\delta q_0 = \begin{cases} -Q_{sat} & (-q_{0k} - \kappa d_k) < -Q_{sat} \\ Q_{sat} & (-q_{0k} - \kappa d_k) > Q_{sat} \\ -q_{0k} - \kappa d_k & otherwise. \end{cases} \qquad (19)$$

κ is a control gain, and Q_{sat} is a saturation that must be chosen appropriately.

B. Example of the robot with 3 DOF at the hip

For the previous control law and reference trajectory, with $\kappa = 0.6$, $Q_{sat} = 6°$, and for an initial pose $q_{0i} = 0°$ and $d_i = -0.275m$, the behavior of the robot is illustrated by the following figures. Figure 7(a) shows the evolution of $q_{0,st}$

on the extended restricted Poincaré section. These variables clearly converge to the desired value and the direction of motion is controlled. Figure 8 (a) shows the center of mass position and the position of the feet on the ground. The robot rejoins smoothly the desired path.

C. Example of the robot with 2 DOF at the hip

Now the results are shown for the same task for the robot presented in Figure 1 (a). Even though the model does not include external/internal rotation at the hip, coupling between the rotations in the sagittal and frontal planes can yield a net rotation about the vertical axis from one step to the next; thus control of the direction of the robot is still possible, though the achieved rate of turning is reduced. For the periodic reference trajectory described in [1] and for $\kappa = 0.2$, $Q_{sat} = 5°$, we obtain the behavior of the robot illustrated in Figure 7 (b) and Figure 8 (b). The robot rejoins smoothly the desired path, but the achievable rate of turning is very limited, resulting in a considerably longer distance along the x-axis in order to complete the turn. Clearly, the robot is less maneuverable than the robot with a 3 DOF hip. Since the net yaw rotation is obtained through a large modification of the trajectory, this change also implies a change in the step length and width, and since the steering control strategy is based on (19) which assumes they are constant, poor performance is obtained. It is also interesting to note that the amount of frontal plane sway of the CoM is higher in the robot without external/internal rotation at the hip.
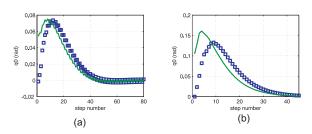

Fig. 7. The evolution of $q_{0,st}$ on the extended restricted Poincaré section. The desired value $(q_{0k} + \delta q_0)$ evolves smoothly and is shown in green solid line.
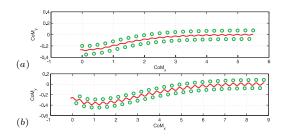

Fig. 8. The evolution of the projection of the center of mass of the robot on the ground is shown by the red line, and the positions of the feet on the ground are shown as green circles. For the same task and the same control methodology, the behavior of the robot with a 3 DOF at the hip shown in (a) and for a 2 DOF hip in (b). Theses figures show clearly that the internal/external rotation of the hip improves the robot's maneuverability.

VI. CONCLUSIONS

Steering has been studied for two 3D bipedal robots with passive ankles. One robot included internal/external (i.e., medial/lateral) rotation at the hip, while the other did not. The method of virtual constraints was used to design a time-invariant, within-stride feedback controller that stabilized all but the yaw motion of each robot. A supplemental event-based (or stride-to-stride) feedback controller was then designed that stabilized the yaw motion. By adjusting the set point of the event-based controller, it was possible to steer the direction of the robot, and even to direct the motion of its center of mass along a given path. This was achieved without designing a specific solution of the model for turning. Instead, the event-based controller modified on-line the final impact configuration and velocity of a path for walking in a straight line. The importance of the internal/external rotation of the hip for turning motions was illustrated via the comparison of the performance of the same control strategy on both robots. The results presented here can be extended to the case of a robot with an actuated ankle.

REFERENCES

[1] C. Chevallereau, J. Grizzle, and C. Shih, "Asymptotically stable walking of a five-link underactuated 3d bipedal robot," *IEEE Transactions on Robotics*, vol. 25, no. 1, pp. 37–50, Fevrier 2009.

[2] Y. Sakagami, R. Watanabe, C. Aoyama, S. Matsunaga, N. Higaki, and K. Fulimura, "The intelligent asimo system overview and integration," in *IEEE/RSJ International Conference on Intelligent Robots and Systems*, 2002, pp. 2478–2483.

[3] S. Kazuo, K. Tsuchiya, and K. Tsujita, "The intelligent asimo system overview and integration," in *IEEE International Conference on Robotics and Automation*, 2004, pp. 3043–3048.

[4] K. Miura, S. Nakaoka, M. Morisawa, H. K., and S. Kajita, "A friction based twirl for biped robots," in *IEEE-RAS International Conference on Humanoid Robots*, 2008, pp. 279–284.

[5] M. Yagi and V. Lumelsky, "Synthesis of turning pattern trajectories for a biped robot in a scene with obstacles," in *IEEE/RSJ International Conference on Intelligent Robots and Systems*, 2000, pp. 1161–1166.

[6] R. Gregg and M. Spong, "Reduction-based control of three-dimensional bipedal walking robots," *International Journal of Robotics Research*, vol. 29, no. 6, pp. 680–702, 2010.

[7] A. D. Ames, R. Sinnet, and E. Wendel, "Three-dimensional kneed bipedal walking: A hybrid geometric approach," in *HSCC*, ser. LNCS, P. Tabuada and R. Majumdar, Eds., vol. 5469. Springer Verlag, 2009, pp. 16–30.

[8] A. Goswami, "Postural stability of biped robots and the foot-rotation indicator (FRI) point," *International Journal of Robotics Research*, vol. 18, no. 6, pp. 523–533, June 1999.

[9] M. Vukobratovic, B. Borovac, D. Surla, and D. Stokic, *Biped Locomotion*. Berlin: Springer-Verlag, 1990.

[10] E. Westervelt, J. Grizzle, C. Chevallereau, J. Choi, and B. Morris, *Feedback Control of Dynamic Bipedal Robot Locomotion*, ser. Control and Automation. Boca Raton: CRC Press, June 2007.

[11] B. Morris and J. Grizzle, "Hybrid invariant manifolds in systems with impulse effects with application to periodic locomotion in bipedal robots," *IEEE Transaction on Automatic Control*, vol. 54, no. 8, pp. 1751 – 1764, August 2009.

[12] M. Spong and F. Bullo, "Controlled symmetries and passive walking,," *IEEE Transactions on Automatic Control*, vol. 50, no. 7, pp. 1025–1031, July 2005.

[13] J. W. Grizzle, "Remarks on event-based stabilization of periodic orbits in systems with impulse effects," in *Second International Symposium on Communications, Control and Signal Processing*, 2006.

[14] G. Arechavaleta, J. Laumond, H. Hitcheur, and A. Berthoz, "On the nonholonomic nature of human locomotion," *Autonomous Robots*, vol. 25, no. 1-2, pp. 25–35, 2008.